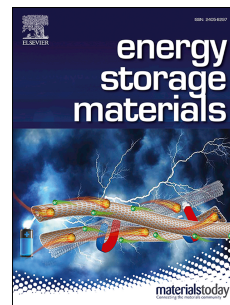


Accepted Manuscript

Cathode electrolyte interface enabling stable Li-S batteries

Xing Xing, Yejing Li, Xuefeng Wan, Victoria Petrova, Haodong Liu, Ping Liu



PII: S2405-8297(19)30844-X

DOI: <https://doi.org/10.1016/j.ensm.2019.06.022>

Reference: ENSM 811

To appear in: *Energy Storage Materials*

Received Date: 25 March 2019

Revised Date: 3 June 2019

Accepted Date: 18 June 2019

Please cite this article as: X. Xing, Y. Li, X. Wan, V. Petrova, H. Liu, P. Liu, Cathode electrolyte interface enabling stable Li-S batteries, *Energy Storage Materials*, <https://doi.org/10.1016/j.ensm.2019.06.022>.

This is a PDF file of an unedited manuscript that has been accepted for publication. As a service to our customers we are providing this early version of the manuscript. The manuscript will undergo copyediting, typesetting, and review of the resulting proof before it is published in its final form. Please note that during the production process errors may be discovered which could affect the content, and all legal disclaimers that apply to the journal pertain.

Cathode electrolyte interface enabling stable Li-S batteries

Xing Xing, Yejing Li, Xuefeng Wan[†], Victoria Petrova, Haodong Liu, and Ping Liu**

Department of Nanoengineering, University of California, San Diego, CA 92093

* E-mail (P. Liu) piliu@eng.ucsd.edu

* E-mail (H.D. Liu) haodong.liu.xmu@gmail.com

Cathode electrolyte interface enabling stable Li-S batteries

KEYWORDS. High Coulombic Efficiency; Cathode Electrolyte Interface; Solid Electrolyte Interface; Li-S Batteries; Li Metal

Abstract

A high-concentration, ether-based electrolyte with LiTFSI and LiNO₃ as the co-salts is proposed, which enables stable cycling of a lithium metal battery using sulfurized polyacrylonitrile (SPAN) as the cathode material. In addition to providing excellent protection for lithium metal anodes by forming the solid electrolyte interface (SEI), the electrolyte promotes the formation of a crystalline cathode electrolyte interface (CEI) on the SPAN surface composed of LiF and LiNO₂. The CEI effectively prevents the formation of soluble polysulfide species and enables stable cycling of the Li/SPAN battery. The benefit of having effective CEI and SEI layers is also demonstrated in Li/SPAN cells with limited lithium supply, which exhibit lithium cycling efficiency values consistent with or exceeding Li/Cu test results, reaching 99.5%. The development of electrolyte chemistries to enable the formation of effective CEI layers is a promising approach to long-life lithium metal batteries.

Introduction

Lithium-sulfur (Li-S) batteries are being extensively studied due to their high theoretical energy density of 2600 Wh/kg and low cost of sulfur[1]. In order to make a long cycle life battery, both electrodes have to be highly reversible and free of side reactions with the electrolyte, and the electrolyte should not promote further parasitic crosstalk between the two electrode reactions[2–4]. There are two classes of Li-S batteries under development.

In the first class, elemental sulfur acts as the active material. Ether-based electrolytes such as LiTFSI-DOL/DME (Lithium bis(trifluoromethanesulfonyl) imide-dioxolane/dimethoxyethane) are preferred over carbonate-based ones because the discharge of sulfur generates polysulfide species, Li_2S_n ($n=2-8$) that react with carbonates but are relatively inert among ethers. The high solubility of polysulfides leads to the widely studied crossover phenomenon, resulting in sulfur (and corresponding capacity) loss at the surface of lithium metal as well as in electrolytes[1]. Addition of an additive, LiNO_3 in particular, has been found to be highly effective in protecting the lithium metal surface from polysulfide attacks allowing for a longer cycle life[5,6]. Indeed, previous work has shown that the polysulfide and the nitrate appear to act synergistically, resulting in a more robust solid electrolyte interface (SEI) on lithium which is rich in Li_2SO_x species[7,8].

A second class of Li-S batteries employs a sulfurized polyacrylonitrile (SPAN)[9]. This material is readily synthesized by reacting elemental sulfur and polyacrylonitrile (PAN), and is electrically conducting, alleviating the need for large amounts of carbon in the electrode as in the case of elemental sulfur. Specific capacities of 400-700 mAh/g are often achieved with a sulfur content of 30-45 wt% [10–13]. Unlike elemental sulfur, SPAN is a highly stable material in carbonate-based electrolyte only, demonstrating a cycle life of up to 1000 cycles [14–16]. SPAN is one of the most stable cathode materials ever identified; the material does not appear to trigger any sulfur dissolution mechanism into the carbonate electrolyte. When used in common ether-based electrolytes, however, the material appears to revert to the solution chemistry of elemental sulfur and polysulfides [17]. The mechanism of SPAN as a cathode material is still a subject of study [18].

While it is highly desirable to employ SPAN due to its cycling stability and potential low cost, the use of carbonate electrolytes creates significant stability issues at the lithium anode. Intensive research using carbonate electrolytes has shown that lithium metal suffers from dendrite growth, low coulombic efficiency (CE) of a maximum of ~92%, and a rapid loss of active lithium. In contrast, ether-based electrolytes, such as LiTFSI-DOL/DME, have consistently shown much higher CE (~98%) and generally dendrite-free

morphology for lithium metal deposits. Highly concentrated ether-based electrolytes have achieved efficiencies of $> 99\%$ [19–21]. This has resulted in recent efforts to identify ether-based electrolytes suitable for the reversible cycling of SPAN[17,22,23].

This work investigates ether-based electrolytes that enable robust cathode electrolyte interface (CEI) and solid electrolyte interface (SEI) layer formations, leading to highly reversible cycling. A promising concentrated ether electrolyte with LiTFSI and LiNO_3 as co-salts is identified for a highly stable Li-SPAN battery. LiNO_3 is hypothesized to encourage the formation of a robust SEI for lithium metal anodes and CEI for SPAN cathodes, while the high salt concentration discourages the dissolution of polysulfide to reduce the consumption of LiNO_3 . Indeed, a CEI that contains crystalline LiF and LiNO_2 is observed for the first time. Finally, a successful Li-SPAN battery with limited lithium supply is demonstrated, which not only confirms the high efficiency cycling of the lithium electrode, but also points to the possibility of high energy density rechargeable batteries.

Experimental section

SPAN material synthesis

All chemicals were purchased from Sigma-Aldrich unless specified otherwise and used without purification. To synthesize SPAN material, elemental sulfur and polyacrylonitrile ($M_w = 150,000$) were hand milled in a ratio of 4:1 to ensure homogeneous mixing. The mixed samples were heated in an argon-filled furnace at 450°C for 6 hours with a ramp rate of $2^\circ\text{C}/\text{min}$, then allowed to cool to room temperature[12].

Electrolyte preparation and solubility tests

Ethylene carbonate (EC), dimethyl carbonate (DMC), 1,3-dioxolane (DOL), 1,2-dimethoxyethane (DME) were purchased from BASF and used as received. The five electrolytes of 1 M LiTFSI/EC-DMC(1:1, v/v),

1 M LiTFSI/DOL-DME(1:1, v/v), 4 M LiTFSI/DOL-DME(1:1, v/v), 1 M LiTFSI/DOL-DME(1:1, v/v) with 0.5 M LiNO₃, and 4 M LiTFSI/DOL-DME(1:1, v/v) with 0.5 M LiNO₃ were prepared by dissolving predetermined amounts of LiTFSI and LiNO₃ salts into mixed solvents and stirred to achieve stable and clear solutions. Solubility tests were performed by adding 0.25 M Li₂S₆ (which corresponds to 0.25 M Li₂S and 1.25 M sulfur) into the respective prepared electrolyte. Photographs of the solutions were taken after 24 hours. The solubility was measured by ultraviolet-visible spectrometry (UV-vis) after 200x dilution with a 1:1 DOL/DME mixture solvent. All the processes were performed in an argon-filled glove box with a water concentration < 1 ppm.

Electrochemical characterizations

Coulombic efficiency of lithium deposition/stripping tests were determined by Li-Cu cells in chosen electrolyte, using LAND battery testers (Wuhan, China). Typically, a constant capacity of lithium (1 mAh/cm²) was deposited on Cu foil at a constant current density 0.5 mA/cm², and then stripped at the same current density to a cut-off voltage of 1.0 V vs Li/Li⁺[24].

SPAN cathode was prepared with SPAN powder, Super-P and PVDF in a ratio of 70:15:15 mixed in N-methyl pyrrolidinone (NMP) solvent and cast on carbon coated Al foil. After drying in a vacuum oven at 80 °C overnight, the SPAN cathode loading was around 1.5 mg/cm². Fixed amount of electrolyte (~34 μL/cm²) is added into each coin cell to guarantee the completely wetting of the separator and electrodes. The electrolyte/SPAN ratio is 22 μL/mg. The cycling performance tests of using excess lithium source were carried out in different electrolytes assembled with lithium discs (MTI, 250 μm thickness) and Celgard separators (Celgard, USA). Galvanostatic charge/discharge was conducted in a fixed voltage range of 1 – 3 V vs. Li/Li⁺ at room temperature with 100 mA/g current density based on SPAN weight.

Limited capacity anodes were prepared electrochemically by using Li-Cu cells. 2 mAh/cm² lithium was deposited onto Cu foil in selected electrolyte at a current density of 0.1 mA/cm²[25]. After deposition, the

cells were disassembled to separate the anode. The anodes were rinsed with ~10 ml of solvent; the cell deposited with 1 M LiTFSI/EC-DMC (1:1, v/v) electrolyte was rinsed with DMC and the cell deposited with 4 M LiTFSI/DOL-DME (1:1, v/v) + 0.5 M LiNO₃ electrolyte was rinsed with DME. Rinsed anodes were dried in vacuum and then coupled with SPAN cathode in the same electrolyte as that used for the lithium depositing cell. The following galvanostatic charge/discharge was conducted in a fixed voltage range of 1 – 3 V vs. Li/Li⁺ at room temperature with 100 mA/g current density based on SPAN weight.

Structure characterizations

The morphologies of the cycled lithium anode surface were characterized using scanning electron microscopy (FEI Quanta 250 SEM) coupled with an energy dispersive X-ray spectrometer (EDS) to determine the chemical composition of the samples. The crystal structures of the cycled cathode surface were examined by X-ray diffraction (XRD) and acquired using a Bruker D2 phaser diffractometer with a Bragg-Brentano θ -2 θ geometry and a Cu K α source ($\lambda = 1.54 \text{ \AA}$). Samples were sealed inside the glovebox with Kapton tape and scanned at a rate of $0.02^\circ \text{ s}^{-1}$. Micrographs were recorded on a field emission gun (FEG) JEM-2100F cryo-transmission electron microscopy (TEM), equipped with a OneView camera and operated at 200 keV. The TEM samples were loaded onto the cooling holder inside glovebox and transferred to the TEM system with continuously flowing argon gas. The images were taken when the temperature of samples reached about 100 K.

Results and Discussion

Four electrolyte compositions are chosen to facilitate the examination of the effect of LiNO₃ addition and salt concentration in Li-SPAN cell; their electrochemical performance is shown in Figure 1a. The cell with the 1 M LiTFSI electrolyte shows rapid capacity degradation, where only 66.5% capacity remains

after 20 cycles. The coulombic efficiency (CE), defined as the ratio of discharge capacity to charge capacity immediately before the step, is less than 50%. This instability is in sharp contrast to the materials outstanding cycling stability in 1 M LiTFSI in EC/DMC with negligible capacity decay over 100 cycles along with close to 100% CE (Figure S1). In the dilute ether electrolyte, the voltage profiles are also different. The Li-SPAN cell only shows a sloped voltage plateau in the discharging and charging voltage profile as shown in Figure S1. However, in the voltage profile of 1 M LiTFSI ether-based electrolyte cell (Figure 1b), there is a voltage plateau at ~ 2.1 V during discharge indicating that the active material displays a behavior similar to that of elemental sulfur[1]. This leads to the well-known shuttle effect which manifests as both irreversible sulfur loss from SPAN cathode due to polysulfide dissolution and as low coulombic efficiency due to reactions between lithium and polysulfides on the anode surface[6]. SPAN exhibits an ultrahigh charge capacity of ~ 2300 mAh/g in the 1 M LiTFSI electrolyte as a consequence of the shuttle effect[1–3,8]. The dissolved low order polysulfides was oxidized to high order polysulfides, which diffuse to anode surface and get reduced back to low order polysulfides by lithium metal, causing this apparent high capacity during charge.

Increasing electrolyte concentration to 4 M leads to a reduced rate in capacity decay (81.2% after 20 cycles), although the capacity retention is still far inferior to that observed in carbonate electrolytes. The voltage profile in Figure 1b no longer shows the distinctive plateau corresponding to the elemental surface redox chemistry. However, CE values are below 99% for the first 20 cycles, indicating the presence of irreversible reactions. The CE reaches over 99.4% after 20 cycles, indicating that the polysulfide shuttle effect is significantly suppressed.

The addition of LiNO_3 is found to have a more significant impact on capacity retention and CE. In the 1 M LiTFSI + 0.5 M LiNO_3 cell, CE increases to close to 100% after 23 cycles and capacity retention is 84.2% after 100 cycles. When 4 M LiTFSI is used in combination with 0.5 M LiNO_3 , cell performance is further improved, achieving 89.4% capacity retention after 100 cycles and a stable CE of 100% after only 6 cycles. As has been previously reported[8], the presence of LiNO_3 can effectively stabilize the lithium

anode surface, via the in-situ formation of a SEI layer, which inhibits the shuttle effect and improves CE. The presence of polysulfide in the solution might actually act synergistically to improve the efficacy of the layer[26]. Noticeably, the ~2.1 V plateau during discharge is also eliminated even in a 1 M LiTFSI electrolyte solution in the presence of LiNO₃ as shown in Figure 1b. A possible explanation is that LiNO₃ suppresses the formation of polysulfides from the SPAN cathode during cycling, which is carefully examined later.

In order to understand the respective roles of LiNO₃ and high salt concentration in determining cell performance, we first analyzed their impact on the lithium metal electrode cycling performance and established that a combination of high salt concentration and LiNO₃ additive enables highly stable lithium metal cycling with good Coulombic efficiency.

The CE tests for lithium metal plating/stripping in different concentrations of electrolytes are performed at a current density of 0.5 mA/cm² and a capacity of 1 mAh/cm² in Li-Cu cells and the results are shown in Figure S2. Also included for comparison are the CE results of the carbonate-based electrolyte (1 M LiTFSI - EC/DMC). The carbonate-based electrolyte has an average CE of 91.6% over 40 cycles, similar to previous reports[21]. The low CE reflects the high reactivity between lithium and the organic carbonates[4,27]. The 1 M LiTFSI ether electrolyte has a CE value averaging around only 80%, even worse than the carbonate. However, raising the salt concentration to 4 M leads to an average CE of 95.3%. With the LiNO₃ additive, high average CEs are achieved in both 1 M (98.1%) and 4 M (98.0%) ether-based electrolytes, suggesting that the LiNO₃ plays a critical role in enabling high efficiency lithium metal cycling[28,29].

We next examine how the electrolyte composition affects polysulfide dissolution. 0.25 M Li₂S₆ is dissolved in the four electrolytes described in Figure 1. Figure S3a shows a high solubility of polysulfide in dilute DOL/DME electrolyte as indicated by the dark-brown color. In contrast, the light-yellow color in concentrated DOL/DME indicates a much lower solubility. To further quantify the solubility, UV-Vis spectra of the solutions are obtained as shown in Figure S3b. The signals were taken after the solutions

were diluted by 200x. The absorption peaks at 475, 420, and 617 nm correspond to S_6^{2-} , S_4^{2-} , and S_3^- , respectively[30]. Based on the calibration curves shown in Figure S3c and d, the calculated concentration of polysulfide in 1 M LiTFSI - DOL/ DME is 0.2312 M, which is consistent with the starting solution of 0.25 M. However, after raising the LiTFSI concentration to 4 M, the solubility drops to only 0.0041 M, clearly demonstrating the effective suppression of polysulfides dissolution. By adding 0.5 M $LiNO_3$ into the concentrated electrolyte, polysulfide solubility is further reduced to 0.0017M. We hypothesize that the reduced solubility is due to Le Châtelier's principle of solubility, although a systematic study using molecular dynamics calculation would help to reveal the actual solution structure, a subject of future study. Therefore, it is concluded that both LiTFSI and $LiNO_3$ help suppress dissolution of polysulfides effectively.

Post-mortem analysis of the cells after cycling is then performed in order to better understand the underlying mechanism. The morphologies of cycled lithium metal anode surface in Li-SPAN cells are evaluated with SEM. As shown in Figure S4, in 1 M LiTFSI electrolyte, non-dendritic lithium metal is observed but the uniformity is poor and voids are clearly present. However, in the concentrated electrolyte with $LiNO_3$ addition, lithium metal particles are big, uniform and highly compact. EDS in Figure S5 confirms that a combination of high salt concentration and $LiNO_3$ leads to the lowest sulfur accumulation on the anode surface, which is consistent with effective polysulfide dissolution suppression and the protective function of $LiNO_3$.

XPS measurements are carried out to further characterize the chemical composition of the respective cycled lithium anode surface. In S_{2p} spectra Figure S6, the double peaks at 167.9 eV and 161.3 eV are assigned to Li_2SO_x and Li_2S/Li_2S_2 based on previous reports[5,6]. The major difference in the spectra in Figure S6a and S6b is the intensity of Li_2S/Li_2S_2 peaks. The addition of $LiNO_3$ greatly reduces the amount of sulfides on the anode surfaces. Previous work has established that Li_2S/Li_2S_2 can be oxidized by NO_3^- into Li_2SO_x on the lithium surface, which is a more effective conducting SEI component in Li-S batteries[31]. This observation is consistent with the results of N1s spectra (Figure S7b). The $Li_2N_xO_y$ and

$\text{Li}_2\text{N}_2\text{O}_2$ peaks confirm the reduction products from LiNO_3 . In the 4M LiTFSI electrolyte, both $\text{Li}_2\text{S}_2/\text{Li}_2\text{S}$ and Li_2SO_x peaks decrease, indicating fewer polysulfides migrate from cathode to anode. The addition of LiNO_3 produces the least amount of sulfides on the anode surface. Therefore, the concentrated electrolyte with LiNO_3 produces less sulfur-containing and more conductive components on the lithium anode surface, which is consistent with SEM-EDS results.

The surface structure of the cathode is then examined after cycling. Figure 2 shows the S2p XPS results obtained on as-harvested electrodes. The double peaks at around 164.8eV are assigned to the C-S and S-S bonds in the SPAN material based on previous reports[16]. The addition of LiNO_3 , however, appears to reduce the signal, indicating that the SPAN is likely covered with a protection layer. This is most evident for the electrode tested in 1 M LiTFSI with LiNO_3 (Figure 2b) where the signals from the SPAN material are completely absent. To confirm this hypothesis, the samples were ion etched and examined again. The results (Figure 3) show an increase of the peak intensities for every electrode, with the electrode cycled in LiNO_3 -based electrolyte experiencing the most significant increase. The S2p spectra also reveals that the surface of the cathode is populated with Li_2SO_x and $\text{Li}_2\text{S}/\text{Li}_2\text{S}_2$ species as well. Comparing Figure 2a and b, the addition of LiNO_3 in 1 M ether electrolyte leads to greatly reduced sulfide ($\text{Li}_2\text{S}/\text{Li}_2\text{S}_2$) to sulfate (Li_2SO_x) ratios. A similar conclusion can be reached when comparing Figure 2c and d for concentrated salt solutions. Thus, the $\text{Li}_2\text{S}/\text{Li}_2\text{S}_2$ components are oxidized by LiNO_3 into Li_2SO_x components on the surface of the cathode, leading to the formation of a CEI layer. Furthermore, this CEI layer has N containing species as well, as shown by the N1s spectra in Figure S8.

We then use TEM to further examine the surface structure of the cathode cycled in 4M LiTFSI with LiNO_3 addition. SPAN itself is an amorphous material as shown in Figure S9. After cycling, a surface layer is observed with a thickness of ~27 nm (Figure 3a). The presence of lattice fringes indicate that the surface layer is crystalline. Selected area electron diffraction (SAED) identifies the phases to be LiF and LiNO_2 . To further confirm this finding, XRD measurements are taken of the electrode. Surprisingly, weak but clearly visible peaks are obtained (Figure 3d) which index to LiF and LiNO_2 . Our XPS, TEM, and

XRD results confirmed the presence of LiNO_2 in the CEI layer, which is a reduction product of LiNO_3 . Previous work has shown LiNO_3 is reduced at below 1.6 V. Although LiNO_2 has solubility in ether, the high salt concentration employed in the current study has promoted its precipitation on the SPAN cathode surface. This is the first time a CEI layer has been directly observed and identified on a SPAN cathode. The presence of the CEI layer is essential to enabling stable cycling of SPAN in ether-based electrolytes, including in dilute solutions where polysulfide solubility is high. This protection mechanism explains our observation in Figure 1b that the polysulfide discharge plateau at ~ 2.1 V and the shuttle effect are absent when the electrolyte contains 0.5 M LiNO_3 . The CEI prevents the discharge products of SPAN from being exposed to large amounts of the electrolyte and effectively suppresses the formation of soluble polysulfides.

It is thus shown that the 4 M LiTFSI with 0.5 M LiNO_3 in DOL/DME electrolyte enables stable Li-SPAN cells by suppressing polysulfide dissolution and forms protective layers on both the cathode and the anode. Its effect on high efficiency Li metal cycling, however, is not examined by the test results shown in Figure 1, where a 250 μm thick lithium metal anode is used. Within the 100 cycles, the supply of active lithium does not determine capacity retention. Rather, the data confirms that SPAN can cycle reversibly in this ether-based electrolyte with good coulombic efficiency. The performance of a cell is then evaluated where the lithium anode has a limited capacity so that consumption of lithium will eventually lead to capacity fade. This testing methodology is also mandated by the desire to design high energy density cells in which a large amount of excess lithium is both costly and detrimental to cell energy density. A capacity of 2 mAh/cm^2 of lithium was electrochemically deposited on Cu current collectors in both carbonate-based (1 M LiTFSI - EC/DMC) and ether-based (4 M LiTFSI - DOL/DME with LiNO_3) electrolytes to serve as limited-capacity lithium anodes. Based on the first cycle efficiency of Li-Cu cells shown in Figure S2, the expected active lithium capacity deposited (C_d) on Cu foil was 1.85 mAh/cm^2 in carbonate electrolyte and 1.89 mAh/cm^2 in ether electrolyte. These lithium anodes were then reassembled in coin cells with the same respective electrolytes as the ones used for lithium deposition but now with

SPAN as the cathodes. For both electrolytes, the limited lithium full cell had an initial discharge capacity of 745-755 mAh/g based on SPAN weight (Figure 4b). This indicates that the amount of Li^+ stripping from the anode during the initial discharge process is the same for both cells. The irreversible transformation during the first lithiation cycle is a well-known phenomenon although unexplained as shown by 1st discharge curves in Figure 4b[9,10], which caused another 0.2-0.3 mAh/cm² capacity (C_1) loss based on the mass loading (m) of 1.5 mg/cm². After the irreversible formation cycle, the estimated capacity ratio between the negative lithium and the positive SPAN electrodes are 2.01 and 1.85 for the two cells, respectively.

As shown in Figure 5a, the ether-based electrolyte enables far more stable cycling than the carbonate, maintaining 427.4 mAh/g after 100 cycles while the capacity of the cell with carbonate electrolyte degraded to zero in 60 cycles. However, both capacity loss profiles show a change in slope as a function of cycle number. The initial slow decay primarily reflects the loss of capacity of the cathode since excess lithium is available. In other words, the cells are cathode limited. After a certain number of cycles when the excess lithium was consumed, the cells become anode limited. The slope of the decay curve reflects the active lithium loss rate.

In the carbonate-based electrolyte, the excess lithium appears to have been consumed after 20 cycles when acceleration of capacity loss is accompanied by a deteriorating efficiency. At this point, the measured cathode capacity is 460 mAh/g (C_r), when the total capacity for the anode and the cathode are balanced. The lithium cycling efficiency can be calculated using the following equation:

$$CE_{Li} = 1 - \frac{C_c/(n-1)}{\bar{S}_c * m} \quad \text{Eq. 1}$$

Where n is cycle number, \bar{S}_c is the average specific capacity of the cathode, m is the areal mass loading of the cathode, and C_c is the consumed lithium capacity. C_c can in turn be calculated by

$$C_c = C_d - C_1 - C_r \quad \text{Eq. 2}$$

where C_d is deposited lithium capacity, C_1 is first cycle irreversible capacity and C_r is the remaining capacity. For the carbonate-based electrolyte cell, C_c is calculated to be 0.89 mAh/cm² based on Eq.2 for the first 20 cycles, and CE_{Li} is determined to be 93.9% based on Eq.1, given \bar{S}_c is 495 mAh/cm². A similar calculation is performed a for the ether-based electrolyte. C_c for 60 cycles is 0.85 mAh/cm² and CE_{Li} is 98.2%, given \bar{S}_c is 525 mAh/cm². Both calculated CE values based on data from the cathode limited region are consistent with measured values in Li-Cu cell. In the anode limited region, the cycle number and capacity deterioration have a power law relationship. In this case, CE_{Li} can be estimated using the equation below:

$$CE_{Li} = \frac{n_2 - n_1}{n_2} \sqrt{\frac{S_{c,n2}}{S_{c,n1}}} \quad \text{Eq. 3}$$

where $S_{c,n}$ is the specific capacity of the n^{th} cycle. Based on Eq.3, the CE_{Li} is calculated to be 91.2% between 30th and 50th cycle when the cell is operated in the lithium-limited region in carbonate-based electrolyte. In contrast, the corresponding CE_{Li} for the concentrated ether electrolyte is 99.5 % between the 70th and 90th cycle. The high lithium cycling efficiency during the full cell tests indicate the formation of a stable SEI layer on the anode surface. Moreover, it also demonstrates that a robust CEI layer forms on the cathode surface, inhibiting the side reactions of lithium metal with polysulfides which might have migrated from cathode.

Conclusions

In summary, we report a concentrated ether-based electrolyte with LiNO₃ as a co-salt for stable-cycling Li-SPAN batteries. While the high concentration helps to reduce polysulfide solubility, the role of LiNO₃ is more critical. It participates in the formation of protective layers on both the anode (SEI) and the cathode (CEI). Most remarkably, a crystalline CEI layer is directly observed by TEM and identified by SAED and XRD. This observation helps explain the finding that addition of LiNO₃ even aids in

suppressing polysulfide dissolution in a dilute ether-based electrolyte (1M LiTFSI). We note that such a protection mechanism is likely more effective on SPAN rather than on common S/C composite cathodes due to the much smaller volume change. Finally, we conclusively demonstrate the impact of high efficiency lithium cycling in a Li/SPAN cell with limited lithium supply. Our work shows the benefits of developing electrolyte compositions for the formation of both SEI and CEI coatings for rechargeable lithium metal batteries. For the Li/SPAN cell, ether-based electrolytes provide a promising pathway towards a long-life, low cost technology.

Acknowledgement

This work was supported by the Office of Vehicle Technologies of the U.S. Department of Energy through the Advanced Battery Materials Research (BMR) Program (Battery500 Consortium) under Contract No. DE-EE0007764.

Data Availability Statement:

The raw/processed data required to reproduce these findings cannot be shared at this time as the data also forms part of an ongoing study.

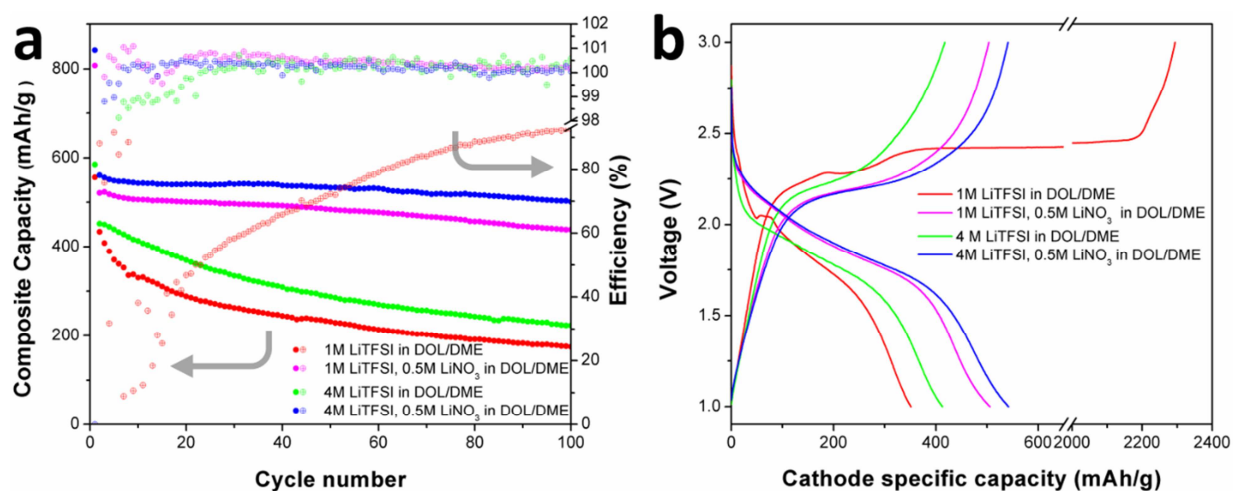


Figure 1. Evaluation of Li-SPAN cell performance with great excess capacity lithium anode. (a) Cycling performance at a current density of 100 mA/g, and (b) 10th discharge and charge voltage profiles of SPAN cathode with lithium anode in different electrolyte.

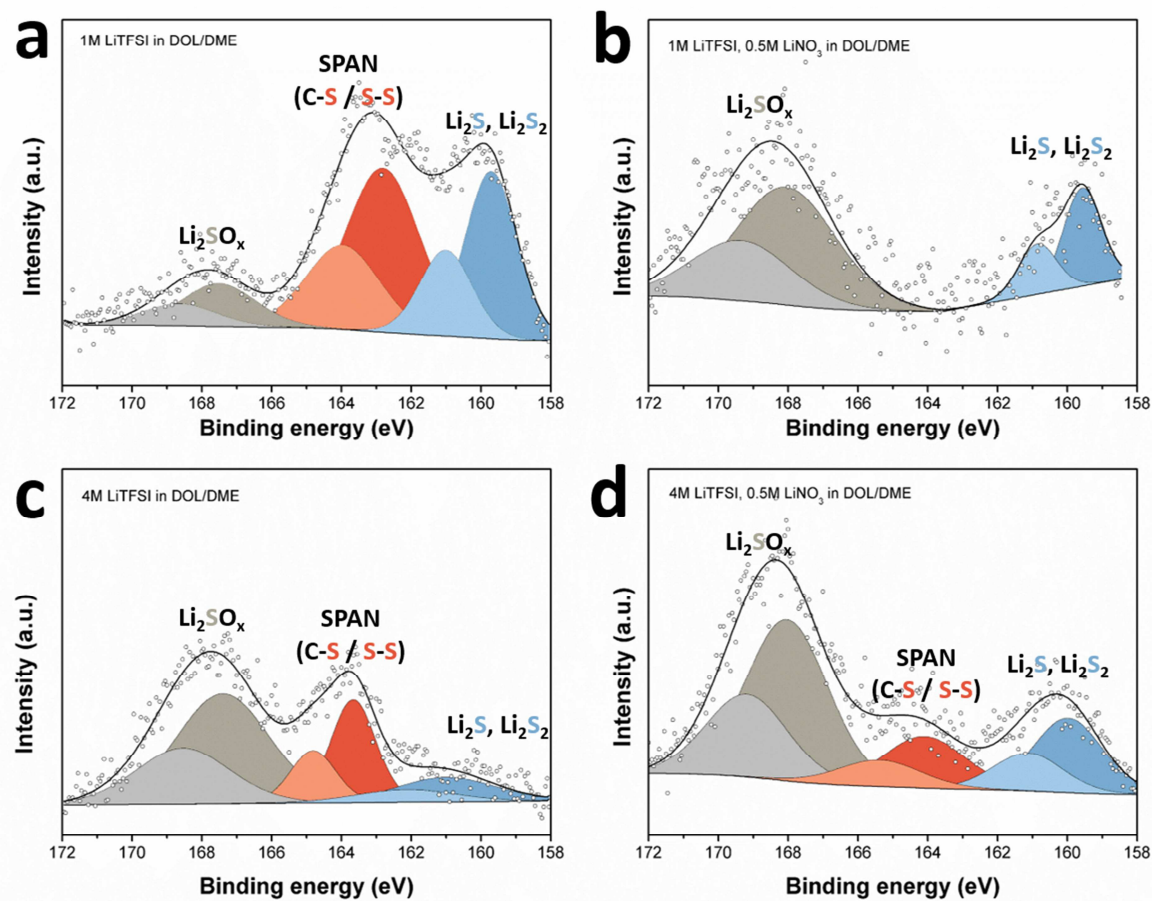


Figure 2. CEI composition identification of the SPAN cathode. XPS S2p spectra of SPAN cathode surface cycled in (a) 1 M LiTFSI in DOL/DME, (b) 1 M LiTFSI and 0.5 M LiNO_3 in DOL/DME, (c) 4 M LiTFSI in DOL/DME, (d) 4 M LiTFSI and 0.5 M LiNO_3 in DOL/DME.

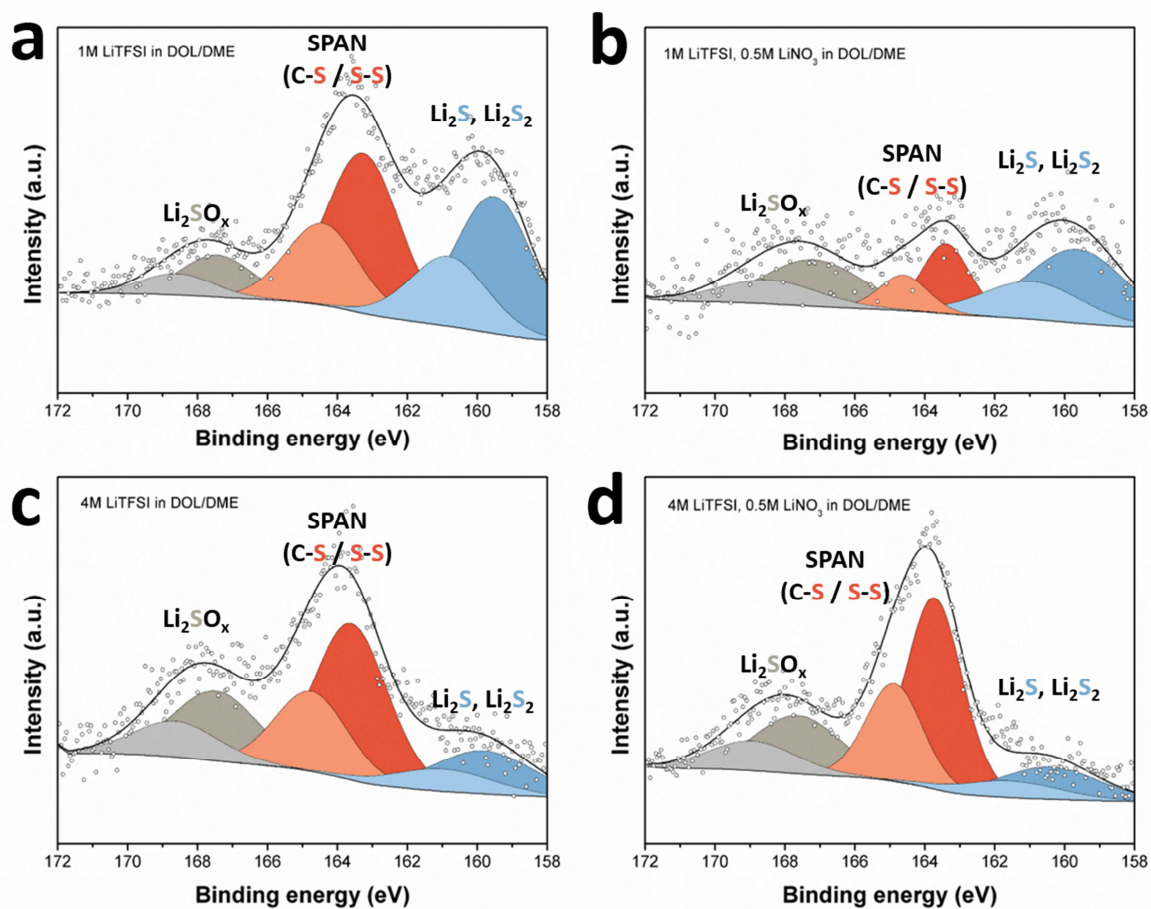


Figure 3. CEI composition identification of SPAN cathode surface after etching. XPS S_{2p} spectra of ion etched cycled SPAN cathode surface in (a) 1 M LiTFSI in DOL/DME, (b) 1 M LiTFSI and 0.5 M LiNO_3 in DOL/DME, (c) 4 M LiTFSI in DOL/DME, (d) 4 M LiTFSI and 0.5 M LiNO_3 in DOL/DME. The etching condition was 10 keV for 300s.

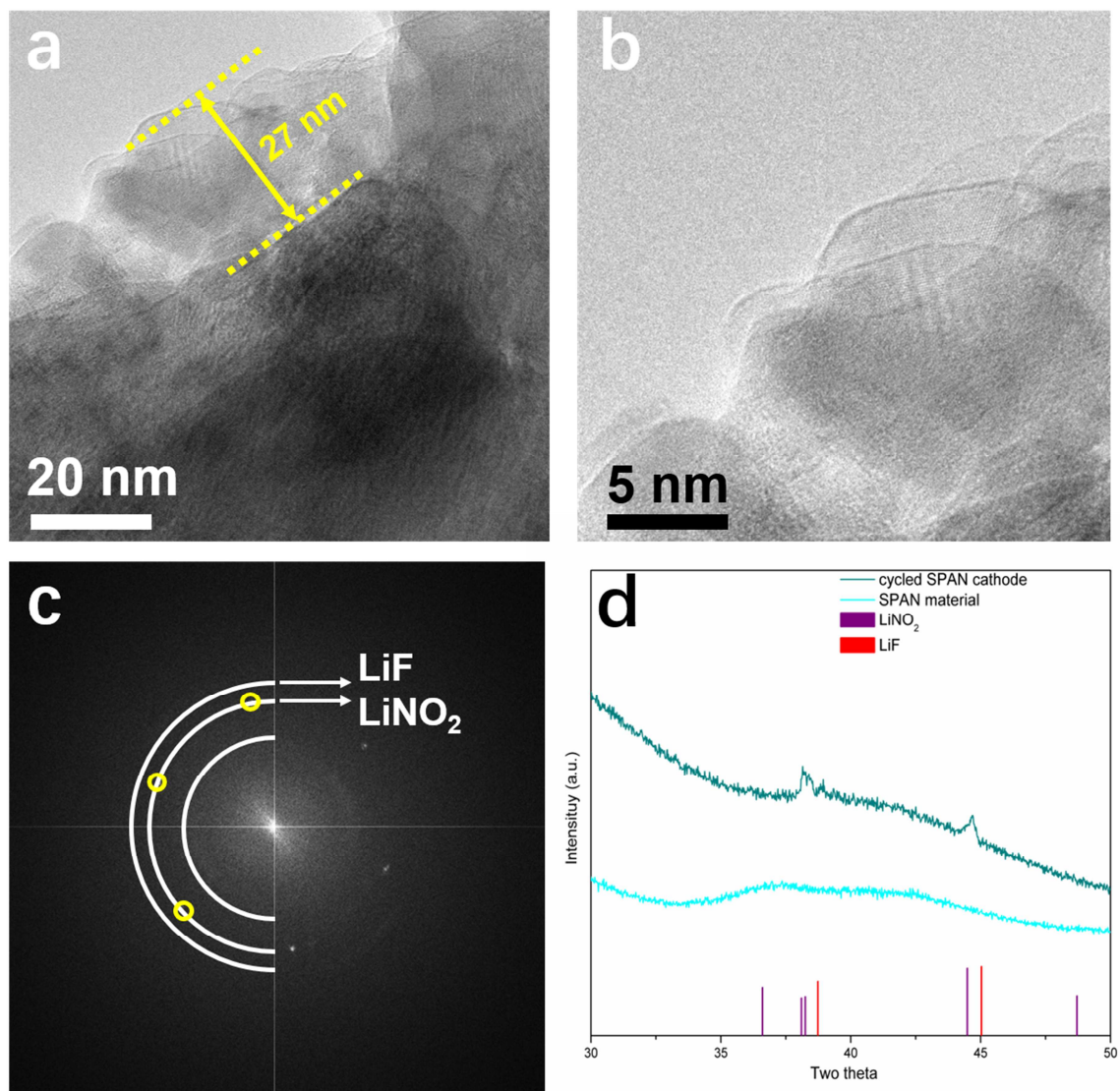


Figure 4. CEI layer structure observation and identification. (a) Cryo-TEM images of SPAN covered with a CEI layer; (b) expanded view of image in (a) near the surface region; (c) selected area electron diffraction (SAED) image and (d) XRD spectra of SPAN cathode after 10 cycles with 4M LiTFSI and 0.5M LiNO₃ in DOL/DME electrolyte.

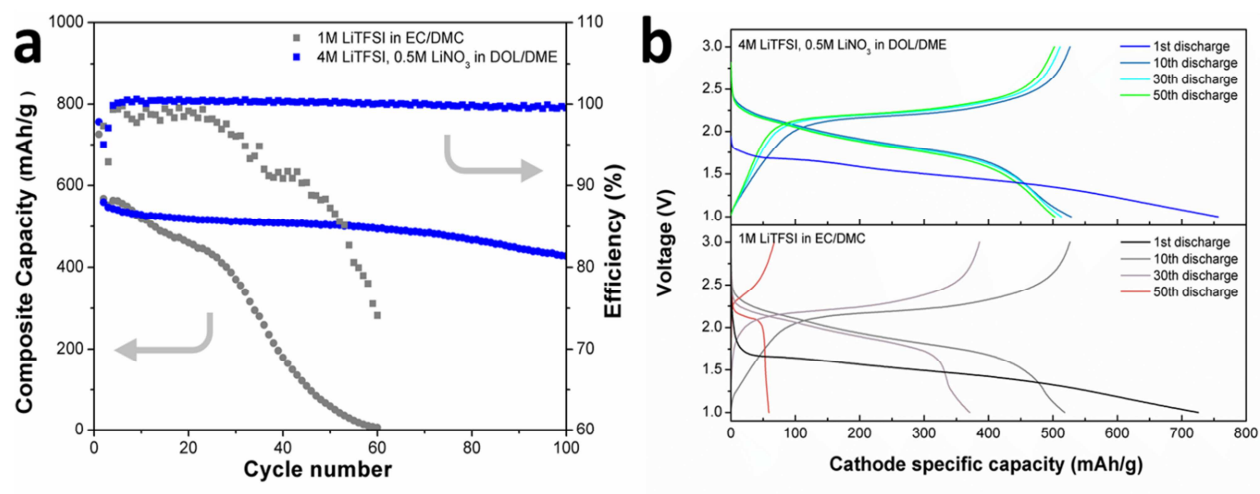


Figure 5. Evaluation of full cell performance with limited lithium capacity anode. (a) Cycling performance at a current density of 100 mA/g, and (b) 10th, 30th, 50th discharge and charge voltage profiles of SPAN cathode with deficient lithium anode in different electrolyte.

- [1] A. Manthiram, Y. Fu, S.H. Chung, C. Zu, Y.S. Su, Rechargeable lithium-sulfur batteries, *Chem. Rev.* 114 (2014) 11751–11787. doi:10.1021/cr500062v.
- [2] R. Kumar, J. Liu, J.Y. Hwang, Y.K. Sun, Recent research trends in Li-S batteries, *J. Mater. Chem. A.* 6 (2018) 11582–11605. doi:10.1039/c8ta01483c.
- [3] T. Ould Ely, D. Kamzabek, D. Chakraborty, M.F. Doherty, Lithium–Sulfur Batteries: State of the Art and Future Directions, *ACS Appl. Energy Mater.* 1 (2018) 1783–1814. doi:10.1021/acsaem.7b00153.
- [4] Y. He, Z. Chang, S. Wu, H. Zhou, Effective strategies for long-cycle life lithium-sulfur batteries, *J. Mater. Chem. A.* 6 (2018) 6155–6182. doi:10.1039/c8ta01115j.
- [5] W. Li, H. Yao, K. Yan, G. Zheng, Z. Liang, Y.M. Chiang, Y. Cui, The synergetic effect of lithium polysulfide and lithium nitrate to prevent lithium dendrite growth, *Nat. Commun.* 6 (2015) 1–8. doi:10.1038/ncomms8436.
- [6] S. Xiong, K. Xie, Y. Diao, X. Hong, Characterization of the solid electrolyte interphase on lithium anode for preventing the shuttle mechanism in lithium-sulfur batteries, *J. Power Sources.* 246 (2014) 840–845. doi:10.1016/j.jpowsour.2013.08.041.
- [7] S.S. Zhang, A new finding on the role of LiNO₃ in lithium-sulfur battery, *J. Power Sources.* 322 (2016) 99–105. doi:10.1016/j.jpowsour.2016.05.009.
- [8] S.S. Zhang, Role of LiNO₃ in rechargeable lithium/sulfur battery, *Electrochim. Acta.* 70 (2012) 344–348. doi:10.1016/j.electacta.2012.03.081.
- [9] J. Wang, J. Yang, C. Wan, K. Du, J. Xie, N. Xu, Sulfur composite cathode materials for rechargeable lithium batteries, *Adv. Funct. Mater.* 13 (2003) 487–492. doi:10.1002/adfm.200304284.
- [10] S.S. Zhang, Sulfurized Carbon: A Class of Cathode Materials for High Performance Lithium/Sulfur Batteries, *Front. Energy Res.* 1 (2013) 1–9. doi:10.3389/fenrg.2013.00010.
- [11] J. Wang, Y.S. He, J. Yang, Sulfur-based composite cathode materials for high-energy rechargeable lithium batteries, *Adv. Mater.* 27 (2015) 569–575. doi:10.1002/adma.201402569.
- [12] S. Wei, L. Ma, K.E. Hendrickson, Z. Tu, L.A. Archer, Metal-Sulfur Battery Cathodes Based on PAN-Sulfur Composites, *J. Am. Chem. Soc.* 137 (2015) 12143–12152. doi:10.1021/jacs.5b08113.
- [13] X. He, Y. Wang, C. Wan, C. Jiang, J. Wang, J. Ren, Electrochemical characteristics of sulfur composite cathode materials in rechargeable lithium batteries, *J. Power Sources.* 138 (2004) 271–273. doi:10.1016/j.jpowsour.2004.06.032.
- [14] J. Wang, Y. Guo, J. Yang, J. Zhou, Y. Nuli, Z. Chen, C. Liang, A compatible carbonate electrolyte with lithium anode for high performance lithium sulfur battery, *Electrochim. Acta.* 282 (2018) 555–562. doi:10.1016/j.electacta.2018.06.093.
- [15] W. Wang, Z. Cao, G.A. Elia, Y. Wu, W. Wahyudi, E. Abou-Hamad, A.H. Emwas, L. Cavallo, L.J. Li, J. Ming, Recognizing the Mechanism of Sulfurized Polyacrylonitrile Cathode Materials for Li-S Batteries and beyond in Al-S Batteries, *ACS Energy Lett.* 3 (2018) 2899–2907. doi:10.1021/acsenergylett.8b01945.
- [16] R.K. Zenn, K. Müller, S. Warneke, M. Frey, R.E. Dinnebier, M.R. Buchmeiser, A. Hintennach, Easily Accessible, Textile Fiber-Based Sulfurized Poly(acrylonitrile) as Li/S Cathode Material: Correlating

- Electrochemical Performance with Morphology and Structure, *ACS Energy Lett.* 2 (2017) 595–604. doi:10.1021/acseenergylett.7b00009.
- [17] J. Zhou, Y. Guo, C. Liang, L. Cao, H. Pan, J. Yang, J. Wang, A new ether-based electrolyte for lithium sulfur batteries using a S@pPAN cathode, *Chem. Commun.* 54 (2018) 5478–5481. doi:10.1039/c8cc02552e.
- [18] S.S. Zhang, Understanding of sulfurized polyacrylonitrile for superior performance lithium/sulfur battery, *Energies.* 7 (2014) 4588–4600. doi:10.3390/en7074588.
- [19] J.T. Lee, Y. Zhao, S. Thieme, H. Kim, M. Oschatz, L. Borchardt, A. Magasinski, W. Il Cho, S. Kaskel, G. Yushin, Sulfur-infiltrated micro- and mesoporous silicon carbide-derived carbon cathode for high-performance lithium sulfur batteries, *Adv. Mater.* 25 (2013) 4573–4579. doi:10.1002/adma.201301579.
- [20] L. Suo, Y.S. Hu, H. Li, M. Armand, L. Chen, A new class of Solvent-in-Salt electrolyte for high-energy rechargeable metallic lithium batteries, *Nat. Commun.* 4 (2013) 1–9. doi:10.1038/ncomms2513.
- [21] R. Miao, J. Yang, Z. Xu, J. Wang, Y. Nuli, L. Sun, A new ether-based electrolyte for dendrite-free lithium-metal based rechargeable batteries, *Sci. Rep.* 6 (2016) 2–10. doi:10.1038/srep21771.
- [22] S. Ma, P. Zuo, H. Zhang, Z. Yu, C. Cui, M. He, G. Yin, enhanced electrochemical performance for room- temperature sodium / potassium sulfur batteries †, (2019) 5267–5270. doi:10.1039/c9cc01612k.
- [23] X. Chen, L. Peng, L. Wang, J. Yang, Z. Hao, J. Xiang, K. Yuan, Y. Huang, B. Shan, L. Yuan, J. Xie, Ether-compatible sulfurized polyacrylonitrile cathode with excellent performance enabled by fast kinetics via selenium doping, *Nat. Commun.* (n.d.) 1–9. doi:10.1038/s41467-019-08818-6.
- [24] P. Liu, H. Liu, Q. Yan, H.-D. Lim, H. Zhou, X. Xing, Y.S. Meng, X. Wang, Structure and Solution Dynamics of Lithium Methyl Carbonate as a Protective Layer For Lithium Metal, *ACS Appl. Energy Mater.* 1 (2018) 1864–1869. doi:10.1021/acsaem.8b00348.
- [25] K. Yan, Z. Lu, H.W. Lee, F. Xiong, P.C. Hsu, Y. Li, J. Zhao, S. Chu, Y. Cui, Selective deposition and stable encapsulation of lithium through heterogeneous seeded growth, *Nat. Energy.* 1 (2016). doi:10.1038/NENERGY.2016.10.
- [26] W. Li, H. Yao, K. Yan, G. Zheng, Z. Liang, Y.M. Chiang, Y. Cui, The synergetic effect of lithium polysulfide and lithium nitrate to prevent lithium dendrite growth, *Nat. Commun.* 6 (2015) 1–8. doi:10.1038/ncomms8436.
- [27] H. Liu, H. Zhou, B.S. Lee, X. Xing, M. Gonzalez, P. Liu, Suppressing Lithium Dendrite Growth with a Single-Component Coating, *ACS Appl. Mater. Interfaces.* 9 (2017) 30635–30642. doi:10.1021/acsaami.7b08198.
- [28] H. Liu, X. Yue, X. Xing, Q. Yan, J. Huang, V. Petrova, H. Zhou, P. Liu, A scalable 3D lithium metal anode, *Energy Storage Mater.* 16 (2019) 505–511. doi:10.1016/j.ensm.2018.09.021.
- [29] B.D. Adams, E. V. Carino, J.G. Connell, K.S. Han, R. Cao, J. Chen, J. Zheng, Q. Li, K.T. Mueller, W.A. Henderson, J.G. Zhang, Long term stability of Li-S batteries using high concentration lithium nitrate electrolytes, *Nano Energy.* 40 (2017) 607–617. doi:10.1016/j.nanoen.2017.09.015.

- [30] M.U.M. Patel, M. Gaberscek, R. Dominko, R. Demir-Cakan, M. Morcrette, J.-M. Tarascon, Li-S Battery Analyzed by UV/Vis in Operando Mode, *ChemSusChem*. 6 (2013) 1177–1181. doi:10.1002/cssc.201300142.
- [31] S.W. Chien, M.B. Sullivan, M.-F. Ng, C. Zhou, Z. Liu, T.S.A. Hor, A. Yu, L. Zhou, D. Geng, Y. Zong, N. Ding, J. Yang, Building better lithium-sulfur batteries: from LiNO₃ to solid oxide catalyst, *Sci. Rep.* 6 (2016) 1–10. doi:10.1038/srep33154.